Periodic density functional embedding theory for complete active space self-consistent field and configuration interaction calculations: Ground and excited states

Thorsten Klüner,[a] Niranjan Govind,[b] Yan Alexander Wang,[c] and Emily A. Carter
Department of Chemistry and Biochemistry, University of California, Los Angeles, California 90095-1159

(Received 3 August 2001; accepted 3 October 2001)

We extend our recently reported embedding theory [J. Chem. Phys. **110**, 7677 (1999)] to calculate not only improved descriptions of ground states, but now also localized excited states in a periodically infinite condensed phase. A local region of the solid is represented by a small cluster for which high quality quantum chemical calculations are performed. The interaction of the cluster with the extended condensed phase is taken into account by an effective embedding potential. This potential is calculated by periodic density functional theory (DFT) and is used as a one-electron operator in subsequent cluster calculations. Among a variety of benchmark calculations, we investigate a CO molecule adsorbed on a Pd(111) surface. By performing complete active space self-consistent field, configuration interaction (CI), and Møller–Plesset perturbation theory of order n (MP-n), we not only were able to obtain accurate adsorption energies via local corrections to DFT, but also vertical excitation energies for an internal ($5\sigma \rightarrow 2\pi^*$) excitation within the adsorbed CO molecule. We demonstrate that our new scheme is an efficient and accurate approach for the calculation of local excited states in bulk metals and on metal surfaces. Additionally, a systematic means of improving locally on ground state properties is provided. © *2002 American Institute of Physics.* [DOI: 10.1063/1.1420748]

I. INTRODUCTION

Experimental and theoretical investigations of elementary molecule–surface interaction events such as adsorption, diffusion, and surface chemical reactions provide fundamental insight into various phenomena, extending from heterogeneous catalysis to materials degradation and growth, and on to surface photochemistry. One prototype extensively studied because of its role especially in catalysis, is the interaction of carbon monoxide with transition metal surfaces. A great amount of experimental data has been obtained for CO adsorption on metals, including binding energies (via thermal desorption spectroscopy or microcalorimetry), electronic structure (via photoemission spectroscopy), vibrational frequencies (via high resolution electron energy loss or infrared spectroscopies), and preferred adsorption sites (via, e.g., low energy electron diffraction). In many cases, a microscopic interpretation of the experimental results benefits from state-of-the-art simulations. Representative papers are mentioned in Ref. 1, with a focus on the particular system chosen for investigation in this paper, which is adsorption of CO on Pd(111).

It is currently possible to calculate ground state properties such as adsorption energies, vibrational frequencies, and equilibrium geometries of adsorbate–substrate systems from first principles. Such calculations are far more demanding than the corresponding ones in the gas phase due to the presence of the surface. *Ab initio* calculations for small molecules in the gas phase often can predict bond dissociation energies and reaction energy barriers with an accuracy of about 0.05 eV (chemical accuracy), but this requires an accurate treatment of electron correlation [e.g., by means of coupled cluster (CC) theory or multireference single and double excitation configuration interaction (MRSDCI)]. Unfortunately, these traditional quantum chemistry methods exhibit a highly nonlinear scaling of the computational effort when the system size is increased. Thus, in calculations of adsorbate-surface interactions only a small part of the semi-infinite surface can be taken into account explicitly or, alternatively, a more approximate theory has to be used. Density functional theory (DFT) within the Kohn–Sham (KS) formalism using approximate exchange-correlation functionals and periodic supercell models is probably the most successful approximate theory for bulk materials, surfaces, and interfaces. It has a favorable scaling behavior with respect to the system size and is a ''first principles'' method in the sense that it uses no input from experiment as other semi-empirical methods do. We still prefer to distinguish DFT from *ab initio* (i.e., traditional quantum chemical) methods, since in DFT the exact exchange-correlation functional is unknown and the results obtained sometimes depend strongly on the approximate functional used. Despite recent developments in the design of new exchange-correlation functionals,[2] DFT in general suffers from this ambiguity.

[a]Present address: Fritz-Haber-Institut der Max-Planck-Gesellschaft, Faradayweg 4-6, 14195 Berlin, Germany.
[b]Present address: Accelrys, 9685 Scranton Road, San Diego, California 92121-3752.
[c]Present address: Department of Chemistry, University of British Columbia, Vancouver, British Columbia, Canada V6T 1Z1.

Once the exchange-correlation functional has been chosen, it is not possible to improve a given result by applying a well-defined hierarchy of methods including more and more electron correlation. This systematic improvement is possible in traditional quantum chemistry, though, where Hartree–Fock (HF) theory serves as a first approximation and static and dynamical correlation effects are introduced via multiconfiguration self-consistent field (MCSCF) or complete active space SCF (CASSCF) and CC or MRSDCI, respectively.

The second main drawback of DFT is that, in contrast to *ab initio* theory, the calculation of wave functions and energies for electronic excited states is less well established. Time-dependent DFT (TDDFT) (Ref. 3) and the GW approximation to the self-energy[4] are promising techniques, but a systematic treatment of condensed matter excited electronic states (especially localized ones) and excited state potential energy surfaces (PES) is not available, especially given that exchange-correlation functionals have been designed for—and/or take as input—ground state densities.[3(b)] TDDFT is based on linear response (LR) theory, with its attendant limitations, e.g., excited states involving multiconfigurational character will be poorly described, as will any states that differ markedly (beyond the LR regime) from the KS ground state. It is also unclear whether residual spin contamination present in the ground state KS determinant will carry over within LR response to spin contaminated excited state solutions. Single particle Green's function approaches within DFT and the GW approximation[4(a)] yield observables for $N_e \rightarrow N_e \pm 1$ transitions, i.e., they are comparable to photoemission or inverse photoemission experiments, but do not yield excitation energies that conserve the number of electrons. Very recently, first principles optical spectra for delocalised band states and for molecules have been calculated using 1- and 2-particle Green's functions derived from DFT.[4(b)] These do correspond to calculations of excited states that conserve particle number. Also recently, semiconductor and insulator band gaps close to experimental values were obtained using a semiempirical DFT functional (B3LYP).[5] This should be regarded as fortuitous, since the experimental band gaps are derived from photoemission/inverse photoemission experiments or optical absorption measurements, where the former measure energy differences between states that do not conserve particle number and where the latter measures energy differences that involve an excitation that does conserve particle number. By contrast, the theoretical band gap reported in these studies is the difference between two orbital energies for the neutral system. These values are not directly comparable, as the theory ignores many-body relaxation effects present in each of the experimental measurements. Moreover, the B3LYP functional, which mixes in some Hartree–Fock exchange, cannot be applied to metals, as Hartree-Fock solutions for such systems are unstable (e.g., exhibiting artificial charge density waves and the density of states at the Fermi surface diverges).[6] Alternatively, quantum Monte Carlo (QMC) (Ref. 7) has been applied in order to estimate delocalized band excitation energies based on explicitly correlated wave functions.[8(a)] A promising approach for insulators and semiconductors has been reported by Bartlett and co-workers,[8(b)] where the band gaps for polymers are markedly improved compared to HF or DFT by using periodic second order perturbation theory. A recently proposed method for calculating the special case of nondegenerate excited singlet states in a Kohn–Sham formalism,[9] based on Slater transition state theory and related schemes,[10] should not be regarded as a solution. This method solves for a wave function (and its associated energy) that is not a spin eigenfunction and therefore cannot be expected to provide accurate excited state properties.

For studying localized phenomena on surfaces, *ab initio* embedded clusters may be more appropriate descriptions than supercell DFT models. However, the validity of the cluster approach depends on the electronic structure type of the solid. For covalent materials, cluster models show some dependence on the size of the cluster used; however, the localized electronic structure of covalent solids suggests that with proper ''embedding'' or termination of the cluster (e.g., tying off dangling bonds with hydrogen atoms), such models can be quite accurate (see, e.g., Ref. 11). For ionic systems with a localized electronic structure, small clusters can give accurate results for adsorption geometries and energies, if the long-range electrostatic interaction of the adsorbate and the surface is simulated by a point charge field. Furthermore, such embedded cluster models can be used for a successful calculation of electronic excited states of adsorbate–surface systems, which lays the foundation of a microscopic understanding of surface spectroscopy and photochemistry. Only recently has the basic mechanism of the most simple photochemical reaction (laser-induced desorption of small molecules adsorbed on oxide surfaces) been clarified by extensive CI embedded cluster calculations, where a cluster was embedded in a point charge array to mimic the long-range Madelung field. It was possible to construct multidimensional potential energy surfaces for the ground and representative excited electronic states, which could be used in subsequent time-dependent wave packet calculations.[12]

Few calculations for models of adsorbate excited states on metal surfaces have been reported before this work,[13] since an embedding scheme for systems with delocalized electronic structure is by no means straightforward. Finite metal clusters without any embedding do not retain the long-ranged delocalized electronic structure, and hence results for interactions with adsorbates tend to vary drastically with cluster size.[14] Thus the need for such embedding schemes for metals has made ground state embedded cluster calculations for metals and metal surfaces an active area of research.[15(a),15(b)] An extensive overview of the literature in this field was given in our recent publications,[13,16] where we introduced[17] a new embedding theory, which efficiently bridges the gap between periodic DFT and conventional *ab initio* theory. In this paper, we report on recent technical improvements of our theory (e.g., extension to CASSCF and CI embedding) and on the extension of applications of the method to localized electronic excited states. Such adsorbate-on-metal excited states have been modeled previously using embedded cluster models and CI,[15(a)] but these previous calculations did not treat the background as an infinite periodic crystal [i.e. either cluster-in-cluster or ''dipped adcluster'' embedding[15(a)]]. Alternative approaches to excited

states in the condensed phase [e.g., GW theory (Ref. 4) and TDDFT (Ref. 3)] are meant for delocalized bandlike excited states or isolated molecules; to our knowledge the method presented here provides the only (complementary) approach to accurately determine excited states of an isolated adsorbate or impurity.[18]

The paper is organized as follows: A brief review of the general features of our embedding theory and the extension to CASSCF, CI, and excited states is given in Sec. II. The calculational details on the cluster and periodic slab models used in our study are provided in Sec. III. Results of calculations for the benchmark system CO/Pd(111) appear in Sec. IV. We offer conclusions and perspectives for further improvements in Sec. V.

II. THEORETICAL MODEL

A. Formulation

In our embedding theory, the total system is partitioned in two regions. Region I denotes the region of interest (e.g., the adsorption site), where accurate quantum chemical cluster calculations (HF, CASSCF, CI or MP-n) are performed. The periodically infinite background is referred to as region II. With this partitioning, the total energy E_{tot} is defined formally as

$$E_{\mathrm{tot}}=\langle\Psi_{\mathrm{tot}}|\hat{H}_{\mathrm{I}}+\hat{H}_{\mathrm{II}}+\hat{H}_{\mathrm{INT}}|\Psi_{\mathrm{tot}}\rangle=E_{\mathrm{I}}+E_{\mathrm{II}}+E_{\mathrm{INT}}, \quad (1)$$

where $\hat{H}_{\mathrm{INT}}$ and E_{INT} denote the Hamiltonian and energy of interaction between regions I and II, and where $\hat{H}_{\mathrm{I}}$, $\hat{H}_{\mathrm{II}}$ and E_{I}, E_{II} refer to the Hamiltonian and energy within regions I and II, respectively. The key quantity of our embedding theory is the interaction energy, since the presence of region II influences region I solely by the interaction Hamiltonian. In a DFT framework, the interaction energy functional can be written as follows:

$$E_{\mathrm{INT}}=T_S^{\mathrm{INT}}+E_{\mathrm{NE}}^{\mathrm{INT}}+E_{\mathrm{XC}}^{\mathrm{INT}}+J^{\mathrm{INT}}+E_{\mathrm{NN}}^{\mathrm{INT}}. \quad (2)$$

T_S, E_{NE}, E_{XC}, J, E_{NN} are the noninteracting kinetic, electron–nuclear attraction, exchange-correlation, Coulomb repulsion, and nuclear–nuclear repulsion energy functionals, respectively. Corresponding expressions exist for the total energy functional and the energy functionals in region I and region II.

According to Eq. (1), the interaction energy functional can be expressed as

$$E_{\mathrm{INT}}=E_{\mathrm{tot}}[\rho_{\mathrm{tot}}]-E_{\mathrm{I}}[\rho_{\mathrm{I}}]-E_{\mathrm{II}}[\rho_{\mathrm{II}}], \quad (3)$$

where each energy functional contains the corresponding terms defined in Eq. (2). The total density $\rho_{\mathrm{tot}}=\rho_{\mathrm{I}}+\rho_{\mathrm{II}}$ is obtained from a periodic DFT calculation and is kept fixed in the entire scheme,[16] which assumes that it is already a good approximation to the exact density. In the future, we plan to lift this requirement, so that the total density will be dynamically updated as well. This basic idea is presented in more detail in Sec. V.

Physically, we desire to know the effect of the infinite surroundings on the region of interest (in terms of how it alters ρ_{I}). This effect manifests itself energetically in terms of E_{INT} and changes in ρ_{I} due to the presence of region II. Therefore, the embedding potential, $\hat{v}_{\mathrm{emb}}$, which describes the effect of the surroundings, is defined[16,17] as the functional derivative of E_{INT} with respect to ρ_{I},

$$\begin{aligned}\hat{v}_{\mathrm{emb}}=\frac{\delta E_{\mathrm{INT}}}{\delta\rho_{\mathrm{I}}}&=\frac{\delta T_S[\rho_{\mathrm{tot}}]}{\delta\rho_{\mathrm{tot}}}-\frac{\delta T_S[\rho_{\mathrm{I}}]}{\delta\rho_{\mathrm{I}}}+\frac{\delta E_{\mathrm{NE}}[\rho_{\mathrm{tot}}]}{\delta\rho_{\mathrm{tot}}}\\&\quad-\frac{\delta E_{\mathrm{NE}}[\rho_{\mathrm{I}}]}{\delta\rho_{\mathrm{I}}}+\frac{\delta E_{\mathrm{XC}}[\rho_{\mathrm{tot}}]}{\delta\rho_{\mathrm{tot}}}-\frac{\delta E_{\mathrm{XC}}[\rho_{\mathrm{I}}]}{\delta\rho_{\mathrm{I}}}\\&\quad+\frac{\delta J[\rho_{\mathrm{tot}}]}{\delta\rho_{\mathrm{tot}}}-\frac{\delta J[\rho_{\mathrm{I}}]}{\delta\rho_{\mathrm{I}}}=\frac{\delta T_S[\rho_{\mathrm{tot}}]}{\delta\rho_{\mathrm{tot}}}-\frac{\delta T_S[\rho_{\mathrm{I}}]}{\delta\rho_{\mathrm{I}}}\\&\quad+(V_{\mathrm{NE}}^{\mathrm{tot}}-V_{\mathrm{NE}}^{\mathrm{I}})+(V_{\mathrm{XC}}^{\mathrm{tot}}-V_{\mathrm{XC}}^{\mathrm{I}})+(V_{\mathrm{H}}^{\mathrm{tot}}-V_{\mathrm{H}}^{\mathrm{I}}),\end{aligned} \quad (4)$$

where V_{NE}, V_{XC}, and V_{H} denote the nuclear–electron, exchange–correlation, and Hartree potentials, respectively. As shown in Eq. (4), the embedding potential arising from region II is the difference between the potentials obtained from the total system and from the cluster in region I. In our current implementation, the terms containing ρ_{tot} are calculated once and for all from a periodic DFT calculation, whereas the terms containing ρ_{I} are updated self-consistently. The only exception is the kinetic energy potential, $\delta T_S[\rho_{\mathrm{I}}]/\delta\rho_{\mathrm{I}}$, which is also kept frozen after being calculated once (see Sec. II C for a detailed discussion).

This definition of the embedding operator has important implications. We approximate the total energy of the system as

$$E_{\mathrm{tot}}\approx E_{\mathrm{tot}}^{\mathrm{emb}}=E_{\mathrm{I}}^{ab}+E_{\mathrm{II}}^{\mathrm{DFT}}+E_{\mathrm{INT}}^{\mathrm{DFT}}, \quad (5)$$

i.e., in the presence of the embedding potential, the total energy is the sum of the *ab initio* energy of region I and the DFT energies of region II and the interaction part, respectively. Rewriting Eq. (5) by adding and subtracting the DFT energy of region I ($E_{\mathrm{I}}^{\mathrm{DFT}}$), we obtain

$$\begin{aligned}E_{\mathrm{tot}}^{\mathrm{emb}}&=E_{\mathrm{I}}^{\mathrm{DFT}}+E_{\mathrm{II}}^{\mathrm{DFT}}+E_{\mathrm{INT}}^{\mathrm{DFT}}+E_{\mathrm{I}}^{ab}-E_{\mathrm{I}}^{\mathrm{DFT}}\\&=E_{\mathrm{tot}}^{\mathrm{DFT}}+(E_{\mathrm{I}}^{ab}-E_{\mathrm{I}}^{\mathrm{DFT}}).\end{aligned} \quad (6)$$

Thus, the embedding theory can be regarded as a local correction to the total DFT energy by an *ab initio* treatment of region I, where E_{I}^{ab} and $E_{\mathrm{I}}^{\mathrm{DFT}}$ are calculated from densities obtained self-consistently in the presence of the embedding potential, $\hat{v}_{\mathrm{emb}}$. This form of the total energy, written as a total energy at a ''lower'' level of theory plus a correction term is reminiscent of that used in QM/MM (Ref. 19) or ONIOM-type[20] schemes. What distinguishes our technique from the latter is the explicit introduction of the interaction of the surroundings with the region of interest via an embedding potential, while the former scheme typically uses only a point charge electrostatic embedding potential.

B. Embedding at different levels of theory

We now describe how $\hat{v}_{\mathrm{emb}}$ enters the *ab initio* calculations in region I for different levels of theory. As a first approximation to an accurate description of region I, we usu-

ally apply Hartree–Fock (HF) theory. The embedding operator enters the HF equations as an additive term to the Fock matrix,[16]

$$\sum_{\nu} (F_{\mu\nu}+M_{\mu\nu})C_{\nu,i}=\epsilon_i\sum_{\nu} S_{\mu\nu}C_{\nu,i}, \tag{7}$$

where $F_{\mu\nu}$ and $S_{\mu\nu}$ denote the Fock- and overlap-matrix elements in the Gaussian atomic orbital basis. ϵ_i and $C_{\nu,i}$ denote the orbital energy and the molecular orbital expansion coefficients for the ith molecular orbital (MO), respectively. $M_{\mu\nu}$ is the matrix representation of the embedding potential in the atomic orbital basis, i.e.,

$$M_{\mu\nu}=\langle\chi_\mu|\hat{v}_{\rm emb}|\chi_\nu\rangle. \tag{8}$$

Since $\hat{v}_{\rm emb}$ contains terms dependent on the density $\rho_{\rm I}$, $M_{\mu\nu}$ is updated in each iteration until self-consistency is achieved. Post-HF perturbative corrections (MP-n) are subsequently calculated using the Hartree–Fock molecular orbitals φ_i obtained in the presence of the embedding potential,

$$\varphi_i=\sum_{\nu} C_{\nu,i}\chi_\nu. \tag{9}$$

This can be done straightforwardly since only the two-electron integrals have to be transformed to the MO-basis in order to obtain the perturbation energies.

The situation for CI and CASSCF is altogether different. In order to calculate the matrix elements of the electronic Hamiltonian, the one-electron embedding integrals have to be transformed as well, i.e.,

$$\langle\varphi_i|\hat{h}+\hat{v}_{\rm emb}|\varphi_j\rangle=\sum_{\mu}\sum_{\nu} C^*_{\mu,i}C_{\nu,j}\langle\chi_\mu|\hat{h}+\hat{v}_{\rm emb}|\chi_\nu\rangle. \tag{10}$$

For a single reference CI calculation, this is done once and for all, after the MO's have been obtained by a preceding HF calculation. For CASSCF calculations, we must do an integral transformation every iteration, since the MO expansion coefficients change as well. Usually then the CASSCF density is used for the construction of the embedding potential.

Of course, CASSCF and CI can be used for the calculation of excited states. However, it is not immediately obvious how to construct an appropriate embedding potential for excited states, since $\hat{v}_{\rm emb}$ is formulated in a DFT-like (and therefore ground-state-like) scheme. Throughout this paper, we use the approximation that ground state embedding operators are applicable to excited state calculations as well. A strategy to improve upon this approximation will be discussed in Sec. V.

C. Embedding potential

Details on the implementation of the individual potential terms in Eq. (4) can be found in a previous paper.[16] Briefly, the Hartree potential was evaluated in Fourier space, as described previously. The exchange-correlation contribution to the embedding potential, $\delta E_{\rm XC}^{\rm INT}[\rho_{\rm I}]/\delta\rho_{\rm I}$, is treated at the LDA or GGA level, consistent with the functional used in the periodic DFT calculation. The LDA potential is accurately calculated on a Becke-type radial grid,[21] whereas the GGA potential is calculated on a uniform grid in real space for convenience. The ion–electron potential, $\hat{v}_{\rm NE}^{\rm II}=\delta E_{\rm NE}^{\rm INT}[\rho_{\rm I}]/\delta\rho_{\rm I}$ is represented by conventional norm-conserving pseudopotentials.[22] The radial part of the pseudopotential was fitted to spherical Gaussians using a nonlinear least-squares optimization. This form of the pseudopotential is necessary for compatibility with the modified version of the HONDO quantum-chemical program package used for the embedding calculations.[23]

We now elaborate on the evaluation of the kinetic energy potential, $\delta T_S^{\rm INT}[\rho_{\rm I}]/\delta\rho_{\rm I}$, since here we use a different approach from that employed in our earlier work. Since the exact kinetic energy density functional (KEDF) is not known (similar to the exchange-correlation functional), an approximate form has to be used. We apply the conventional gradient expansion (CGE) up to second order,[24]

$$T_S^{\rm approx}[\rho]=T_{\rm TF}[\rho]+\tfrac{1}{9}T_{\rm vW}[\rho,\nabla\rho], \tag{11}$$

where

$$T_{\rm TF}[\rho]=\frac{3(3\pi)^{2/3}}{10}\int\rho(\mathbf{r})^{5/3}d\mathbf{r}=C_F\int\rho(\mathbf{r})^{5/3}d\mathbf{r}$$

is the Thomas–Fermi functional and

$$T_{\rm vW}=\frac{1}{8}\int\frac{|\nabla\rho(\mathbf{r})|^2}{\rho(\mathbf{r})}d\mathbf{r},$$

the von Weizsäcker functional. The corresponding approximate kinetic energy potential turns out to be

$$\begin{aligned}\frac{\delta T_S^{\rm approx}[\rho]}{\delta\rho}&=\frac{\delta T_{\rm TF}[\rho]}{\delta\rho}+\frac{1}{9}\frac{\delta T_{\rm vW}[\rho,\nabla\rho]}{\delta\rho}\\&=\frac{5}{3}C_F\rho(\mathbf{r})^{2/3}+\frac{1}{72}\left[\frac{|\nabla\rho(\mathbf{r})|^2}{\rho(\mathbf{r})^2}-2\frac{\nabla^2\rho(\mathbf{r})}{\rho(\mathbf{r})}\right]\\&=V_{\rm TF}+\tfrac{1}{9}V_{\rm vW},\end{aligned} \tag{12}$$

where

$$V_{\rm TF}=\tfrac{5}{3}C_F\rho(\mathbf{r})^{2/3}$$

and

$$V_{\rm vW}=\frac{1}{8}\left[\frac{|\nabla\rho(\mathbf{r})|^2}{\rho(\mathbf{r})^2}-2\frac{\nabla^2\rho(\mathbf{r})}{\rho(\mathbf{r})}\right]$$

denote the Thomas–Fermi and von Weizsäcker kinetic energy potentials, respectively.

Given the total density $\rho_{\rm tot}$ and the *ab initio* density $\rho_{\rm I}$, the evaluation of the interaction kinetic energy potential is now feasible from

$$\frac{\delta T_S^{\rm INT}}{\delta\rho_{\rm I}}=\frac{\delta T_S[\rho_{\rm tot}]}{\delta\rho_{\rm tot}}-\frac{\delta T_S[\rho_{\rm I}]}{\delta\rho_{\rm I}}. \tag{13}$$

Unfortunately, we encountered a severe problem when pseudovalence densities (those densities arising from use of a pseudopotential) are inserted in Eq. (13). The use of pseudopotentials is an intrinsic approximation in many plane-wave-based DFT codes, akin to typical effective core potentials (ECP's) present in many quantum chemistry programs. The effect of the nucleus and core electrons is replaced by a nonlocal pseudopotential (or ECP), which turns

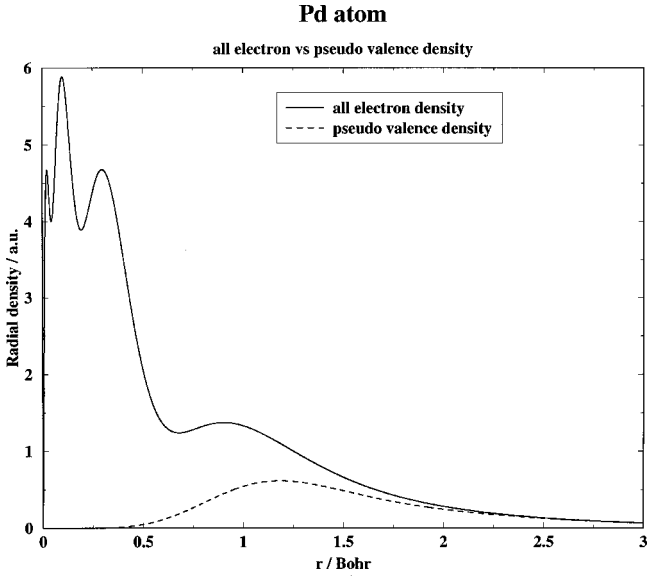

FIG. 1. Pd atom: Radial Kohn–Sham DFT (PW91) densities. Full line: all electron density; dashed line: pseudovalence density. The densities are forced to match at distances larger than $r_c = 2.39$ bohr.

out to be a very good approximation in most applications. For our purposes, however, we found that the von Weizsäcker potential exhibits singularities close to the nuclei if pseudo-valence densities are used for the construction of the kinetic energy potential.

In order to investigate the origin of this phenomenon, we performed atomic calculations where we could calculate these potentials with high accuracy from all-electron and pseudo-valence densities. The Kohn–Sham equations were solved numerically.[25] Figure 1 shows the all-electron radial density $r^2 \cdot \rho(r)$ for a Pd atom and the corresponding pseudo-valence density when norm-conserving pseudopotentials[22] are used. In the valence region, the all-electron and pseudo-valence densities are almost indistinguishable. The all-electron wave function and the pseudovalence wave function are forced to match at distances larger than $r_c = 2.39$ bohr. Because of the pseudopotential, the pseudovalence density rapidly decays to zero in the core region. The calculated kinetic energy potentials for the pseudovalence density are shown in Fig. 2(a). Because of the rapid decay of the density, the gradient-containing terms in the von Weizsäcker potential become artificially large and are even amplified since they are divided by the small density in the core region. This is to be contrasted with the behavior of the all-electron kinetic energy potentials shown in Fig. 2(b), where we see that the Thomas–Fermi potential always dominates the CGE and the von Weizsäcker potential never exhibits singularities.

This pseudopotential artifact mentioned above can be overcome by considering the convergence radius of the conventional gradient expansion. Following Hohenberg and Kohn,[24] the CGE can be applied only if $|\nabla\rho|/k_F\rho \ll 1$, with k_F being the Fermi-wave-vector $k_F = (3\pi^2\rho)^{1/3}$. We use a similar condition (based on potentials for convenience) as a truncation criterion for the CGE, i.e.,

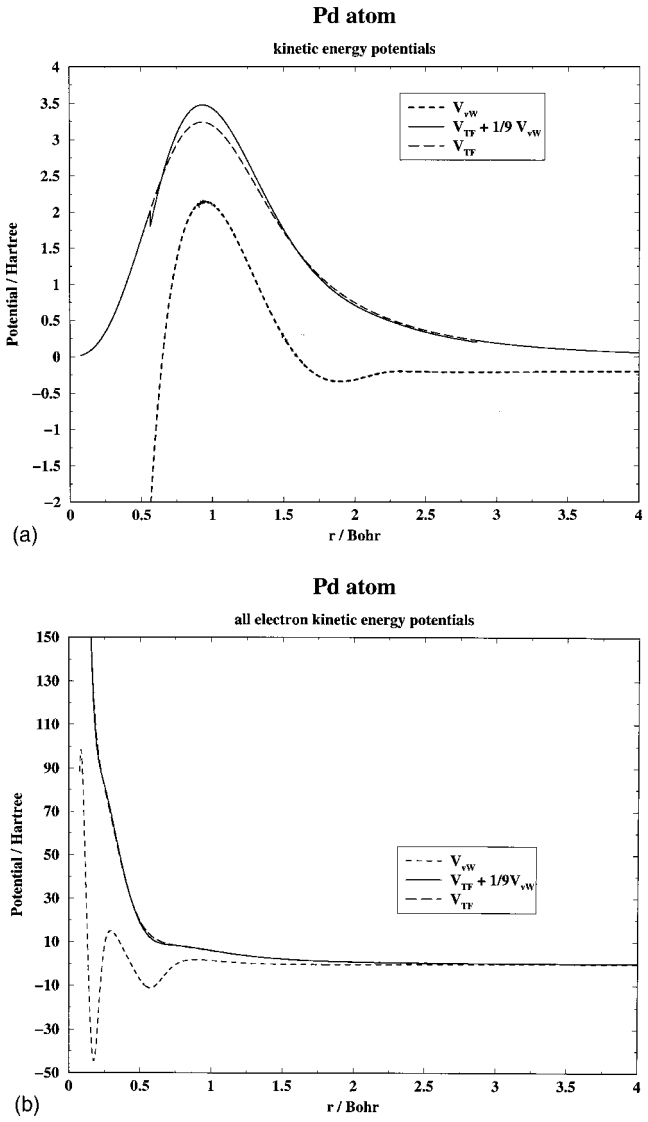

FIG. 2. Pd atom: Kohn–Sham DFT(PW91) kinetic energy potentials obtained from (a) the pseudovalence density and (b) the all-electron density. Full line: locally truncated conventional gradient expansion (CGE) potential (a) or full CGE potential (b); dashed line: von Weizsäcker potential; long dashed line: Thomas–Fermi kinetic energy potential.

$$\frac{\delta T_S^{\text{approx}}[\rho]}{\delta\rho} = \begin{cases} V_{\text{TF}} + \dfrac{1}{9} V_{\text{vW}} & \text{if } \dfrac{V_{\text{vW}}}{V_{\text{TE}}} \leqslant 1 \\ V_{\text{TF}} & \text{if } \dfrac{V_{\text{vW}}}{V_{\text{TF}}} > 1. \end{cases} \tag{14}$$

Numerical tests for the Pd atom show that in practice, this truncation criterion is very similar to the Hohenberg–Kohn condition. The resulting potential for the locally truncated CGE [Eq. (14)] is shown in Fig. 2(a) as well. The potential is now well-behaved close to the nucleus. From Fig. 2(a), it is clear that for small distances and in the asymptotic region, we should use the Thomas–Fermi potential only. For moderate distances, the CGE $T_{\text{TF}} + \frac{1}{9} T_{\text{vW}}$ is applicable. However, close inspection of Fig. 2(a) shows that the locally truncated CGE exhibits kinks at the truncation points. This turns out to be no problem in practice, since in our embedding calculations the kinetic energy potentials due to both ρ_{tot} and ρ_{I} are

calculated on the rather coarse uniform grid in Fourier space (the one used in the periodic DFT calculation). For this reason, these kinks are not resolved.

One further approximation in the construction of the approximate kinetic energy potential was found to be necessary. In Sec. II A, we pointed out that in general all embedding potential terms containing ρ_{tot} are kept frozen, whereas all terms containing ρ_{I} are updated self-consistently. The only exception is $\delta T_S[\rho_{\mathrm{I}}]/\delta\rho_{\mathrm{I}}$, i.e., the kinetic energy potential calculated from the *ab initio* density. We found empirically that a self-consistent update of this term generally yields inferior results compared to a frozen density calculation. In other words, we employ the approximation that $\delta T_S[\rho_{\mathrm{I}}]/\delta\rho_{\mathrm{I}} = \delta T_S[\rho_{\mathrm{I}}^0]/\delta\rho_{\mathrm{I}}^0$, where ρ_{I}^0 denotes the converged *ab initio* density in region I in the absence of the embedding potential, which is usually the initial density in our self-consistent embedding scheme. So, similar to the embedding terms containing ρ_{tot}, $\delta T_S[\rho_{\mathrm{I}}^0]/\delta\rho_{\mathrm{I}}^0$ is calculated once and for all at the beginning of an embedding calculation. While such a procedure seems to be quite arbitrary, it is known in the literature that inserting ''good'' densities into the CGE gives much better kinetic energies than a self-consistent scheme.[26] We assume in the present work that this is true not only for kinetic energy functionals but also for their corresponding potentials.

A crucial test justifying these various approximations will be presented in Sec. IV A.

III. CALCULATIONAL DETAILS

A. Periodic DFT calculation

The first step in our benchmark study of CO on a Pd(111) surface is a periodic DFT calculation, for which the CASTEP program package has been used.[27] We model the Pd(111) surface with a three layer slab containing 8 Pd atoms per layer. Convergence studies with respect to the number of layers show that a three layer slab is sufficiently thick to accurately calculate properties such as adsorption geometries and energies. A CO molecule is placed at an fcc hollow site on one side of the slab corresponding to a coverage of 0.125 monolayers (Fig. 3). The simulation cell, which is periodically repeated in three dimensions, was sufficiently large (5.52 Å×9.55 Å×16.00 Å) so that the interaction between periodic slab images normal to the Pd(111) surface was negligible. In order to obtain an accurate density ρ_{tot}, a plane wave cutoff of $E_{\mathrm{cut}}=700$ eV and a surface Brillouin zone sampling containing 9 special *k*-points was used. As mentioned in Sec. II C, nonlocal norm-conserving pseudopotentials were used to replace the core electrons and nuclei. Since surface relaxation effects were found to be unimportant for the adsorption energy and geometry of CO on the Pd(111) surface,[1,2(a)] the substrate geometry has been chosen to be identical to the experimental bulk lattice constant. However, a full geometry optimization has been performed for the adsorbed CO molecule using the PW91 GGA exchange-correlation functional.[28] From these calculations, we find an adsorption energy of $\Delta E_{\mathrm{slab}}^{\mathrm{DFT}}=-1.71$ eV and a linear geometry defined by the interatomic distances $d(\mathrm{C–O})=1.172$ Å and carbon–surface distance $d(\mathrm{C–S})=1.362$ Å. This is in reasonable agreement with other theoretical and experimental data. Loffreda *et al.*[1] found in a DFT study the optimized distances $d(\mathrm{C–O})=1.189$ Å and $d(\mathrm{C–S})=1.296$ Å. Experimental results are reported to be about $d(\mathrm{C–O})=(1.15\pm0.05)$ Å and $d(\mathrm{C–S})=(1.29\pm0.05)$ Å.[29(a)]

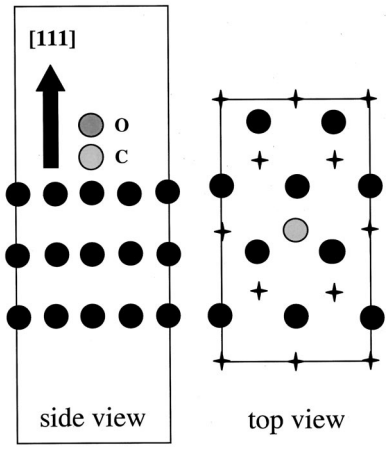

FIG. 3. Pd(111)/CO: the slab model containing 3 Pd layers with 8 atoms per layer. The CO molecule adsorbs at an fcc hollow site with the molecular axis parallel to the surface normal. The stars indicate unoccupied fcc hollow sites.

B. Embedded cluster calculation

The second step in our embedding scheme is a quantum chemical cluster calculation for region I in the presence of the embedding potential. The smallest cluster consists of three Pd atoms of the fcc hollow site (Pd_3) and the CO molecule. The cluster size convergence was studied for excited state calculations by including the three Pd atoms adjacent to the three Pd atoms of the adsorption site, in the second metal layer, resulting in a Pd_6 cluster. All core electrons are replaced by large core ECP's,[29(b),30] and for an accurate description of the valence electrons, a double-zeta basis set turns out to be sufficient.[31] The basis set superposition error (BSSE) for interaction energies is $\leqslant 0.1$ eV in this basis set, as evaluated via the counterpoise correction of Boys and Bernardi.[32] The BSSE is so small that we did not use ghost functions at the atomic sites adjacent to the cluster, which was found to be necessary in our previous work.[16] Note that use of standard quantum chemical ECP's in the cluster calculations introduces an inconsistency in our approach, since Troullier–Martins pseudopotentials[22] have been used in the periodic slab calculations. However, using ECP's in region I was found to yield better results for the properties of interest, especially with respect to vertical excitation energies. In Sec. IV B, we discuss the problem of validity of ECP's and Troullier–Martins pseudopotentials in (any) quantum chemical or DFT calculations of excited states.

All embedded cluster calculations were performed with a modified version of the HONDO quantum chemical program package.[23] We carried out embedded cluster ground state calculations within Hartree–Fock or MP-*n* theory, though of course our newly implemented CASSCF and CI embedding theory could have been employed also.

C. Local correction term for ground state energetics

Once the *ab initio* energy in region I in the presence of the embedding potential, $E_{\mathrm{I}}^{ab}[\rho_{\mathrm{I}}]$, has been calculated, $E_{\mathrm{I}}^{\mathrm{DFT}}[\rho_{\mathrm{I}}]$ must be obtained for the construction of the local correction term, $E_{\mathrm{I}}^{ab}[\rho_{\mathrm{I}}]-E_{\mathrm{I}}^{\mathrm{DFT}}[\rho_{\mathrm{I}}]$, according to Eq. (6). This is performed by calculation of a Kohn–Sham DFT energy expectation value for the converged density ρ_{I}^{ab}, i.e.,

$$E_{\mathrm{I}}^{\mathrm{DFT}}[\rho_{\mathrm{I}}]=E_{\mathrm{I}}^{\mathrm{DFT}}[\rho_{\mathrm{I}}^{ab}]=T_S[\rho_{\mathrm{I}}^{ab}]+E_{\mathrm{NE}}[\rho_{\mathrm{I}}^{ab}]+E_{\mathrm{XC}}[\rho_{\mathrm{I}}^{ab}]+E_{\mathrm{H}}[\rho_{\mathrm{I}}^{ab}]+E_{\mathrm{NN}}. \tag{15}$$

With the exception of $T_S[\rho_{\mathrm{I}}]$, and given a choice of E_{XC}, all terms in Eq. (15) can be evaluated exactly in terms of the density. However, in the evaluation of the kinetic energy functional, the noninteracting kinetic energy,

$$T_S=-\frac{1}{2}\sum_{i=1}^{N}\langle\varphi_i|\nabla^2|\varphi_i\rangle \tag{16}$$

and not the conventional gradient expansion is used to obtain accurate energies. In our current embedding scheme, the orbitals used in Eq. (16) are those obtained in an embedded Hartree–Fock calculation. This has to be regarded as a further approximation, since a rigorous scheme would require construction of an effective Kohn–Sham potential v_{eff} from the density ρ_{I}^{ab}. In a second step, one would solve for the Kohn–Sham orbitals corresponding to this v_{eff}, which in turn would be used in Eq. (16). However, this approximation is expected to be reasonable, since in many cases Hartree–Fock and Kohn–Sham orbitals turn out to be quite similar.[33]

D. Embedded cluster excited state calculations

For the calculation of excited states corresponding to internal CO excitations, we first obtained the MO's in an embedded CASSCF(10/7) calculation, where the 3σ, 4σ, 5σ, 1π, and $2\pi^*$-like orbitals of the CO molecule are included in the active space. To facilitate the identification of the MO's that should be included in the active space, an initial guess wave function corresponding to a large molecule-surface distance ($R=1000$ bohr) was constructed. The well separated MO's were helpful in designing the active space in the subsequent CASSCF calculations, since at very large distances no mixing with Pd MO's occurs.

The embedded CASSCF density matrix was obtained by averaging the density matrices for the electronic ground state and the excited state of interest (in this case the $^1\Pi$-state) for the CO molecule with equal weights. After obtaining the MO's under the influence of the embedding potential, we performed a valence CI calculation with the same active space as in the preceding CASSCF calculation, but now the embedding operators are constructed by using a ground-state-like single determinant reference configuration with the CASSCF MO's. This corresponds to a ground-state embedding potential as pointed out in Sec. II B. Exploratory calculations using nonground-state-like embedding potentials (e.g., excited state density matrices) gave far less consistent results.

Vertical excitation energies for the Pd_3/CO and Pd_6/CO systems are obtained by the calculation of the corresponding eigenvalues of the CI-matrix. This calculation of vertical excitation energies is different from the evaluation of adsorption energies according to Eq. (6). Whereas the calculation of adsorption energies is a local correction to the total DFT energy, the evaluation of vertical excitation energies utilizes the idea of performing CI calculations for a small cluster under the presence of an effective (ground-state-like) embedding potential. In other words, the excitation energies are obtained directly from the energy difference between the embedded *ab initio* total energies for region I, E_{I}^{ab}, for the two states. An extension of this scheme will be discussed in the final section of this paper.

TABLE I. Basis sets for gas phase CO calculations.

Basis I	$4s4p/2s2p+1d(0.8)+1p(0.05)$	$1s$ ECP; SBKJC[a]
Basis II	C: $9s5p1d/4s2p1d+1p(0.034)$ O: $9s5p1d/4s2p1d+1p(0.059)$	DZP+$1p$ Dunning[b]
Basis III	$11s6p3d2f/5s4p3d2f$	aug-cc-pVTZ[c,d]
Basis IV	C: $12s6p3d2f1g/5s4p3d2f1g$ $+1s(0.023)+1p(0.021)+1d(0.015)$ O: $12s6p3d2f1g/5s4p3d2f1g$ $+1s(0.032)+1p(0.028)+1d(0.015)$	cc-pVQZ+$1s1p1d$[d]

[a]Reference 31.
[b]Reference 35.
[c]Reference 36.
[d]Reference 37.

E. Benchmark calculations on gas phase CO

In order to judge the influence of our rather small basis set and the neglect of dynamical correlation effects on vertical excitation energies, we performed extensive benchmark calculations for the CO molecule in the gas phase using the MOLCAS (Ref. 34) and HONDO program packages. The C–O distance used corresponds to the experimental value of 1.128 Å. Various states were calculated using four different basis sets (listed in Table I). The influence of dynamical correlation effects was investigated by extensive MRSDCI calculations. The reference configuration space was generated by CAS(10/8) calculations using the same active orbital space as in the embedded cluster calculations (i.e., the 3σ, 4σ, 1π, 5σ, $2\pi^*$-orbitals), as well as the $6\sigma^*$-MO. This choice of active space is discussed further in the next section. For the largest basis set (basis IV), the CI expansion contains between 6.5 million CSF's [for the $D\,^1\Delta$-state with a CAS(10/8) reference space of 272 CSFs] and 12.5 million CSF's [for the $b\,^3\Sigma^+$-state with a CAS(10/8) reference space of 360 CSFs], resulting in very accurate vertical excitation energies. Details are discussed in Sec. IV.

IV. RESULTS

A. CO/Pd(111): Ground state calculations

1. DFT in DFT embedding

In order to test the general validity of our approach, we first performed a DFT-LDA calculation in region I in the presence of the DFT-LDA embedding potential, for the pure Pd(111) surface, as represented by a Pd_3 cluster embedded in

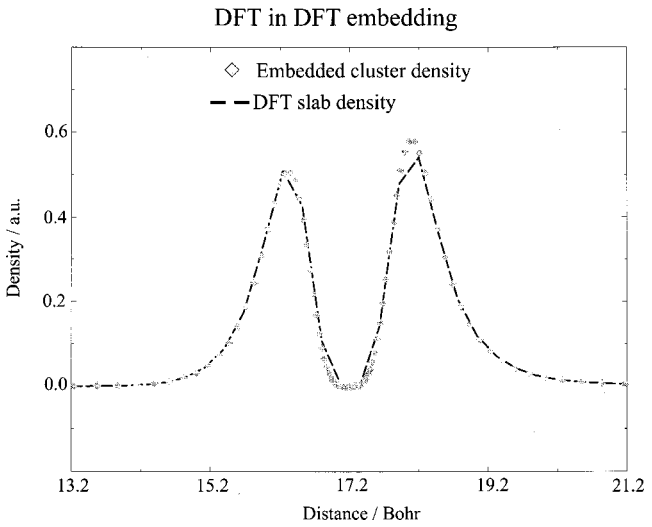

FIG. 4. DFT (LDA) in DFT (LDA) embedding calculation. The diamonds denote a slice of an embedded cluster electron density along a given direction; the dashed line is the same cut through a density obtained from a DFT slab calculation.

the periodic slab described in Sec. III A. According to Eq. (6), such a procedure should simply reproduce the results of the periodic slab DFT calculation. Of course, the correction term in Eq. (6) is zero by construction but all other observables should be identical as well. A comparison of the periodic slab total density with the embedded cluster density in region I along a particular direction (Fig. 4) clearly demonstrates that these densities are virtually identical. Small differences are likely due to the grids used in the embedding (Becke-type) versus the DFT slab (uniform grid). We regard this calculation as a crucial test for our embedding scheme, especially with respect to the choice of our kinetic energy potential (Eq. 14) and the frozen density approximation applied for $\delta T_S[\rho_I]/\delta\rho_I$. It appears both approximations are performing well for the present example, but future studies will show whether these approximations are generally applicable.

2. Embedded versus nonembedded cluster calculations: Adsorption energies

The next step in our study is a comparison of embedded and nonembedded cluster calculations with periodic slab calculations applying different levels of theory. In Table II, we present the results for the adsorption energy, ΔE_B, of CO on Pd(111) using a Pd_3 cluster. The calculations are performed at the adsorption geometry optimized in a periodic slab DFT calculation (Sec. III). Our periodic DFT result ($\Delta E_B = -1.71$ eV) differs from the experimental adsorption energy[38] ($\Delta E_B = -1.47$ to -1.54 eV) by about 0.2 eV. However, in other studies where different slab models, limiting coverages, plane wave cutoffs and pseudopotentials were used, rather different results are reported[2(a)] ($\Delta E_B = -2.07$ eV), even though the same PW91 exchange-correlation functional was employed. This shows the level of variability of results one can expect when performing DFT slab calculations, due to various numerical parameter choices.

TABLE II. Adsorption energy (ΔE_{ads}) for CO on Pd(111).

ΔE_{ads}/eV	Pd_3/CO embedded	Pd_3/CO not embedded
E(HF)	−2.13	−1.75
E(MP-2)	−1.42	−4.55
E(MP-4)	−1.55	−5.03
E_{slab}(PW91)	−1.71 to −2.07[a]	
E_{slab}(LDA)	−2.98	
E(expt.)	−1.47 to −1.54[b]	

[a]Reference 2(a).
[b]Reference 38.

By contrast, nonembedded cluster calculations exhibit severe problems. While nonembedded HF-calculations give fortuitously good results, the Møller–Plesset perturbation series diverges, yielding far too large values for the adsorption energy. The divergence can be traced back to quasidegenerate one-particle energies for the occupied and virtual orbitals resulting in artificially small energy denominators in the MP-n perturbation energy corrections.

The embedded cluster results exhibit a different picture, when the locally truncated CGE for the kinetic energy functionals and the PW91-GGA for the exchange-correlation functionals are applied. The adsorption energies are obtained using Eq. (6), i.e., the local binding energy correction ($\Delta E^{ab\ initio}_{B,\text{region I}} - \Delta E^{\text{DFT}}_{B,\text{region I}}$) is added to the DFT slab binding energy $\Delta E^{\text{DFT}}_{B,\text{slab}}$. Hartree–Fock theory overestimates the adsorption energy ($\Delta E_B = -2.13$ eV), but the MP-n series, which in this case does not exhibit convergence problems in the presence of the embedding potential (see Sec. IV C), yields results in excellent agreement with experiment. Actually, the deviation from the experimental value is only on the order of 0.05 eV, which is smaller than the intrinsic errors (basis set, BSSE) in our calculations, and probably smaller than the uncertainty in the experimental value.[38] However, the results have to be regarded with some caution, since the adsorption energy has been calculated at the PW91 DFT equilibrium geometry obtained from a periodic slab model. Since we did not perform a geometry optimization of the embedded cluster, there might be a slight inconsistency between the calculated MP-n adsorption energy and the PW91 geometry. Future studies allowing structural relaxation will clarify this point.

3. Sensitivity to the KEDF choice

A crucial feature of our embedding scheme is the choice of the kinetic energy density functional (KEDF). Since the exact KEDF is unknown (similar to the exact exchange-correlation functional) an ambiguity arises in our theory. However, the choice of the KEDF is not as critical in our embedding theory as it is in orbital-free DFT,[39] since the KEDF enters, e.g., the Hartree–Fock equations only as an effective one-electron operator and is therefore a second-order effect. Of course, the influence of various KEDFs on the results must be investigated. Table III contains adsorption energies using different approximations for the kinetic energy functionals used in the embedding potential. It turns out that the gradient-corrected functionals (CGE) result in much

TABLE III. Adsorption energy Pd_3/CO using different kinetic energy functionals for the embedding potential. E(MP-4)/LDA denotes a MP-4 calculation with a LDA exchange correlation embedding potential. All other energies have been obtained with a PW91 exchange correlation embedding potential.

ΔE_{ads}/eV	$T_{TF}+1/9T_{vW}$	T_{TF}	T_{ZLP}
E(HF)	−2.13	−1.86	−1.92
E(MP-2)	−1.42	−2.13	−2.05
E(MP-4)	−1.55	−2.21	−2.13
E(MP-4)/LDA	−1.98	−2.04	−2.02

more accurate interaction energies on the correlated level compared to the non-gradient-corrected ones [TF, ZLP (Ref. 40)]. The use of gradient-corrected kinetic energy functionals is consistent with the use of a gradient-corrected exchange-correlation functional (PW91), due to the intimate relationship between T_S and E_{XC}.[41] For comparison, we include in Table III MP-4 results where we applied the local density approximation (LDA) to the exchange-correlation functional in the embedding potential together with various kinetic energy functionals. Obviously, LDA gives inferior results throughout the study, which is not surprising, since already the LDA slab result is not at all in good agreement with experiment ($\Delta E_B = -2.98$ eV). In such a case, even our embedding theory cannot compensate for all deficiencies of the local density approximation. It is interesting to note, though, that the MP-4 adsorption energies using a LDA embedding potential seem to be almost independent of the choice of the kinetic energy functional; this is in contrast to the PW91 embedding potential, which exhibits far higher sensitivity to the T_S choice.

In conclusion, our embedding scheme works very well for the calculation of the adsorption energy of CO/Pd(111) at the MP-2 or MP-4 level of theory. We find that gradient corrections for the embedding potential are mandatory to ensure accuracy, both for kinetic energy and exchange-correlation terms in the embedding potential.

B. Benchmark vertical excitation energies for gas phase CO

In order to estimate the accuracy of our embedded cluster excited state calculations (*vide infra*), we investigated the dependence of CO vertical excitation energies on the atomic orbital basis, details of the CASSCF calculations, and the use of ECP's. Energy differences between the $X\,^1\Sigma^+$ ground state and the low-lying $a\,^3\Pi$, $b\,^3\Sigma^+$, $d\,^3\Delta$, $A\,^1\Pi$, and $D\,^1\Delta$ states were calculated, and the influence of dynamical correlation effects was investigated by MRSDCI calculations. The geometry was kept fixed corresponding to the experimental gas phase value of $R_c = 1.128$ Å.[42] Actually, a geometry optimization for the $X\,^1\Sigma^+$ ground state results in a very similar internuclear distance [$R_e = 1.133$ Å, CAS(10/8), basis IV]. Throughout the study, the irreducible representations of the C_{2v} subgroup of the molecular point group $C_{\infty v}$ were used to specify the states of interest. In Table IV, we present excitation energies for the four different basis sets introduced in Sec. III (Table I) together with experimental results from the literature.[43]

1. Size of active space

Using basis I, excitation energies were calculated at the CASSCF level, optimizing the MO's for each state separately. Dynamical correlation effects were neglected. Two active spaces were employed: the CAS(10/8) space introduced in Sec. III and a smaller CAS(6/6) space, which contains only the 4σ, 5σ, 1π, and $2\pi^*$-MO's. Obviously, the CAS(6/6) space is too small to give accurate results, since the difference between the CAS(10/8) and CAS(6/6) can be larger than 1 eV depending on the state (see, e.g., the $X\,^1\Sigma^+ \rightarrow A\,^1\Pi$ transition). Furthermore, using the irreducible representations of the C_{2v} molecular subgroup to specify the state of interest in a CAS(6/6) calculation can result in an energetically wrong ordering of states compared to a CAS(10/8) calculation. For instance, the lowest $^3A_1$ state in a CAS(6/6) calculation corresponds to the $d\,^3\Delta$ state and not to the $b\,^3\Sigma^+$ state as in CAS(10/8). Therefore, we conclude that the size of the active space in our subsequent embedded cluster calculations should be similar to that of a CAS(10/8)

TABLE IV. Vertical excitation energies, ΔE (eV), relative to ground state $X\,^1\Sigma^+$ CO for different basis sets and electron correlation methods ($R_e = 1.128$ Å).

	Basis I		Basis II		Basis III		Basis IV		
State	CAS(6/6)	CAS(10/8)	CAS(10/8)	MRSDCI	CAS(10/8)	MRSDCI	CAS(10/8)	MRSDCI	Experiment[a]
$a\,^3\Pi$	7.36	6.67	6.60	6.31	6.65	6.32	6.65	6.34	6.25
$b\,^3\Sigma^+$	(9.23)[b]	9.15	11.42	11.08	10.66	10.47	10.48	10.36	10.25 8.38 for $a\,^3\Sigma^+$
$d\,^3\Delta$	(10.28)[c]	(10.14)[c]	10.14	9.55	10.12	9.42	10.12	9.43	9.25
$A\,^1\Pi$	10.34 (9.61)[d]	9.26 (9.08)[d]	9.19	8.68	9.23	8.59	9.23	8.60	8.38
$D\,^1\Delta$	11.03	10.78	10.78	10.29	10.72	10.12	10.72	10.13	10.00 8.88 for $I\,^1\Sigma^-$

[a]Reference 43.
[b]State is $d\,^3\Delta$ (Lit: $\Delta E = 9.25$ eV).
[c]State is $e\,^3\Sigma^-$ (Lit: $\Delta E = 9.69$ eV).
[d]State-averaged CASSCF.

calculation. As pointed out in Sec. III, the active space in the embedding calculation contains only seven orbitals, where the $6\sigma^*$-MO is excluded from the active space, resulting in a CAS(10/7) calculation. We find that the inclusion of the $6\sigma^*$-MO is not necessary for the accuracy required in the embedding calculation. As further evidence, the MRSDCI vertical excitation energies for a $X\,^1\Sigma^+ \rightarrow {}^1\Pi$ transition differ only by 0.03 eV (basis IV), depending on the reference space used [CAS(10/7) or CAS(10/8), respectively]. Therefore, the CAS(10/7) calculation is certainly sufficient in the embedded cluster calculations. Nevertheless, our gas phase results may be regarded independently as accurate benchmark calculations of CO vertical excitation energies. For this reason, we also included the $6\sigma^*$-MO in the active space in these gas phase calculations.

2. State-averaged versus state-optimized CASSCF

For the ($X\,^1\Sigma^+ \rightarrow A\,^1\Pi$) excitation, the effect of a state-averaged CASSCF calculation was investigated, since a state-averaging procedure is applied in our embedded cluster calculations. In this procedure, one common set of MO's for both states is obtained by superposition of the corresponding one-particle density matrices with equal weights, i.e.,

$$\Gamma_{\mathrm{av}} = 0.5 \cdot \Gamma_1 + 0.5 \cdot \Gamma_2 . \tag{17}$$

Obviously, the approximate state-averaging reduces the vertical excitation energy slightly compared to the state-optimized results [0.18 eV for CAS(10/8)]. For the excitation of interest in the embedding calculations ($X\,^1\Sigma^+ \rightarrow A\,^1\Pi$), we obtain an energy of 9.08 eV (state-averaged) instead of 9.26 eV (state-optimized).

3. Error due to ECP's

The next point to address is the use of pseudopotentials (ECP's) in excited state calculations, since their construction generally is based on ground-state wavefunctions. In order to investigate this question, Table IV provides a comparison of excitation energies obtained with basis I (using ECP's) and with basis II (no ECP's, but similar valence basis set quality compared to basis I). The accuracy of the results depends strongly on the state under investigation. The application of the ECP approximation turns out to be valid for $a\,^3\Pi$, $A\,^1\Pi$, and $D\,^1\Delta$ states. By contrast, a large error is obtained for the $b\,^3\Sigma^+$ state (2.27 eV). For the $d\,^3\Delta$ state, the results even imply a wrong ordering of states, since the state that is supposed to be the $d\,^3\Delta$ state (in C_{2v} symmetry, a $^3A_2$ state) turns out to be of $e\,^3\Sigma^-$ symmetry. Given the use of pseudopotentials in the DFT slab calculations of CO/Pd(111), we must employ ECP's on the Pd, C, and O atoms in the embedded region for consistency. However, this therefore restricts the excited states which we can expect to study accurately to $A\,^1\Pi$, $a\,^3\Pi$, and $D\,^1\Delta$ states. Furthermore, we found vertical excitation energies obtained with Troullier–Martins pseudopotentials to be less accurate than those obtained by using ECPs. This is not surprising, since the Troullier-Martins pseudopotentials are built within a DFT formalism (unscreened with a DFT exchange-correlation potential) and therefore would not be expected to give accurate results for a CI calculation. As will be shown later, the most interesting transition is the $X\,^1\Sigma^+ \rightarrow A\,^1\Pi$ transition, since contradictory experimental results are discussed in the literature concerning the correct vertical excitation energy.[44–46] For this excitation, the use of ECPs results in a CASSCF excitation energy of 9.26 eV (state-optimized), whereas the use of Troullier–Martins pseudopotentials produces 9.50 eV.

4. MRSDCI calculations: Basis set effects

In Table IV we also report MRSDCI results for basis II, in order to judge the importance of dynamical correlation effects. In general, the inclusion of dynamical correlation tends to reduce the vertical excitation energies for all states under investigation (by 0.3–0.6 eV). This is also true for the larger basis sets III and IV. Furthermore, for all but one state ($b\,^3\Sigma^+$), the DZP basis set (basis II) yields virtually identical results compared to basis III and IV, i.e., the absolute differences are in the order are in the order of 0.05 eV. The increase of basis set quality from TZP to QZP does not change the results. The only exception is the $b\,^3\Sigma^+$ state, which exhibits a slow convergence with basis set size due to its Rydberg-type character. Diffuse functions are essential for an accurate description. Therefore, a larger error is obtained if this state is calculated using basis I or II.

5. Assessment of expected correlation/basis set error in CASSCF embedding

Next, we should compare the state-averaged CAS(10/8) excitation energy obtained with basis I (corresponding to the level of calculation in subsequent embedded cluster studies) with the precise MRSDCI excitation energy using basis IV. As pointed out above, state averaging reduces the vertical excitation energy slightly, as does the inclusion of dynamical correlation effects. State-averaged CAS(10/8)/basis I yields a vertical excitation energy of about 9.08 eV, whereas MRSDCI/basis IV produces 8.60 eV. Thus, an intrinsic overestimation of the vertical excitation energy for the ($X\,^1\Sigma^+ \rightarrow A\,^1\Pi$) transition of about 0.5 eV can be traced back to the basis set limitations, state-averaging, and the neglect of dynamical electron correlation. This error should be kept in mind when our excited state embedded cluster calculations for CO/Pd(111) are compared to experimental values.

Finally, we compare our results for the vertical excitation energies for the gas phase CO molecule with the experimental values of Ref. 43. In general, our MRSDCI results (Table IV) agree very well with the data reported in Ref. 43. The deviations are on the order of only 0.2 eV. However, it should be pointed out that the lowest-lying states in the corresponding C_{2v} subgroup irreducible representations $^3A_1$ and $^1A_2$ are reported to be $a\,^3\Sigma^+$ and $I\,^1\Sigma^-$ states. This is in qualitative disagreement with our calculations, where we find the $b\,^3\Sigma^+$ and $D\,^1\Delta$ to be the lowest states corresponding to the $^3A_1$ and $^1A_2$ irreducible representations. Therefore, we believe the vertical excitation energies for the $a\,^3\Sigma^+$ and $I\,^1\Sigma^-$ states reported in Ref. 43 to be incorrect. Actually, vertical transitions from the ground state equilibrium geometry ($R = 1.128$ Å) into these states address quite repulsive parts of the excited state potential curves, where an accurate assignment may be difficult. However, our MRSDCI/basis

TABLE V. Adiabatic energy difference, ΔE, between the $X\,^1\Sigma^+$ state ($R_e = 1.128$ Å) and two excited states ($a\,^3\Sigma^+$, $I\,^1\Sigma^-$) at their equilibrium interatomic distances.

State	ΔE(MRSDCI)/eV	Experiment[a]
$a\,^3\Sigma^+$ ($R_e = 1.352$ Å)	6.88	6.92
$I\,^1\Sigma^-$ ($R_e = 1.391$ Å)	8.10	8.11

[a]Reference 43.

TABLE VI. Vertical excitation energy for the $^1(5\sigma/1\pi \rightarrow 2\pi^*)$ transition: CASSCF(10/7)/CI.

ΔE/eV	Pd_3/CO	Pd_6/CO
With embedding	9.6	9.8
Without embedding	4.5	(3.1)[a]

[a]Reference 47.

IV results agree very well with the data in Ref. 43 if the energy differences between the $X\,^1\Sigma^+$ and the $a\,^3\Sigma^+/I\,^1\Sigma^-$ states are calculated each at their respective equilibrium distance, i.e., $R_e = 1.352$ Å for the $a\,^3\Sigma^+$ and $R_e = 1.391$ Å for $I\,^1\Sigma^-$. The results reported in Table V exhibit differences with Ref. 43 of less than 0.05 eV.

In conclusion, the calculations reported in this section allow us to estimate the error in vertical excitation energies in subsequent calculations for CO/Pd(111) due to basis set limitations, state averaging and neglect of dynamical correlation. We performed highly accurate MRSDCI benchmark calculations for vertical transitions from the electronic ground state to the low-lying excited electronic states of CO. We expect an overestimation for the $(X\,^1\Sigma^+ \rightarrow A\,^1\Pi)$ transition energy of about 0.5 eV, when these intrinsic approximations are introduced into the subsequent embedding calculations.

C. CO/Pd(111): Vertical excitation energies

As mentioned earlier, beyond accurate calculations of ground state properties such as adsorption energies, our embedding theory enables us to investigate electronic excited states of adsorbates on metal surfaces. In the present study, we investigate vertical excitation energies of CO adsorbed on Pd(111).

Electron energy loss spectroscopy (EELS) is the most common tool available for the experimental determination of vertical excitation energies of molecules on surfaces, but it suffers from poor resolution on metal surfaces and therefore the assignment of particular transitions can be ambiguous. Netzer *et al.*[44] reported an excitation energy for the CO internal $^1(5\sigma/1\pi \rightarrow 2\pi^*)$ excitation to be 13.5 eV. However, EELS results reported by Freund *et al.*[45] and Avouris *et al.*[46] for various analogous systems, such as CO/Fe(110), CO/Ni(100), and CO/Cu(100), attribute a feature in the spectra at about 8.0–9.0 eV to this excitation. Actually, this is very similar to the $(X\,^1\Sigma^+ \rightarrow A\,^1\Pi)$ vertical excitation energy of a CO molecule in the gas phase (see Sec. IV B).

In order to clarify whether CO on Pd(111) is an exception regarding vertical excitation energies or if the assignment by Netzer *et al.* is incorrect, we performed embedded cluster CI calculations using Pd_3/CO and Pd_6/CO clusters (the latter to investigate the cluster size effect).

First of all, appropriate orbitals for the subsequent CI calculations are obtained by CASSCF, where we include the 3σ, 4σ, 5σ, 1π, and $2\pi^*$-orbitals in the active space. This CAS(10/7) active is very similar to the CAS(10/8) space, which is sufficient to obtain accurate excitation energies (see Sec. IV B). A balanced description of both electronic states [the ground state and the $^1(5\sigma/1\pi \rightarrow 2\pi^*)$ excited state] is achieved by constructing state-averaged orbitals according to Eq. (17). The embedding operators are constructed using these state-averaged densities. This procedure ensures that the iteratively updated embedding operators are consistent with the CASSCF energy functional.

After constructing the one-particle space in the presence of the infinite background, we can use these state-averaged MO's for an embedded CI study in which the configuration space is identical to the active space of the preceding CAS(10/7) calculation. However, as pointed out in Sec. III, the embedding operators are now constructed using the ground state closed shell reference configuration. Thus, we assume the ground-state-density-based embedding operators to be appropriate for excited state CI calculations as well. Certainly, this approach must be regarded as a first approximation and future studies have to be performed in order to prove the general applicability of the present scheme. An extension of this strategy to a more rigorous treatment of excited states will be presented in Sec. VI as a perspective.

The results for vertical excitation energies for the transition of interest are reported in Table VI. The geometry of the cluster/adsorbate complex is kept fixed at the ground state values reported in Sec. III. For Pd_3/CO and Pd_6/CO we obtain excitation energies of 9.6 eV and 9.8 eV, respectively. This lends confidence that our results are converged with respect to the cluster size. Our results clearly suggest the assignment of Netzer *et al.*[44] [13.5 eV for the $^1(5\sigma/1\pi \rightarrow 2\pi^*)$ excitation] to be incorrect. As pointed out in the last section, our calculations overestimate the $(X\,^1\Sigma^+ \rightarrow A\,^1\Pi)$ excitation energy by about 0.5 eV due to correlation and basis set limitations.

Taking this error into account, we would predict a vertical $^1(5\sigma/1\pi \rightarrow 2\pi^*)$ excitation energy for CO/Pd(111) of 9.1–9.3 eV, which is in very good agreement with the observations of Freund *et al.*[45] and Avouris *et al.*[46] for analogous systems.

To demonstrate the relevance of an accurate embedding potential, we performed nonembedded cluster calculations as well. As shown in Table VI, the excitation energies are much too small (3.1–4.5 eV). This failure of nonembedded cluster calculations can be traced back to an underestimation of the Pauli-repulsion between the CO $2\pi^*$-orbital and the extended surface in the absence of the embedding potential. The presence of the surface increases the energy of the $2\pi^*$-orbital and consequently also the energy of the $^1(5\sigma/1\pi \rightarrow 2\pi^*)$ excitation. Furthermore, the embedding potential increases the gap between the occupied and virtual orbital energies in general. This results in a much better convergence of the MP-n series in the presence of the embedding operators, since the quasidegeneracies which caused the

divergence of the MP-n series in the absence of the embedding potential (Sec. IV A 2) no longer occur.

V. DISCUSSION AND CONCLUSIONS

In this work, we performed CASSCF and CI calculations on clusters embedded in an extended environment that has been treated at the DFT level using periodic slab models. We have demonstrated its ability to systematically reduce the error in DFT calculations locally for ground states and to accurately calculate localized excited states in a periodically infinite condensed phase. In our density-based embedded cluster approach, an effective one electron embedding operator is constructed from a periodic DFT calculation. In a subsequent quantum chemical cluster calculation, this embedding operator is self-consistently updated.

Our approach has been applied to the well studied adsorbate/substrate system, CO/Pd(111). We were able to accurately calculate the adsorption energy at the MP-4 level of theory. We demonstrated that gradient-corrected exchange-correlation and kinetic energy functionals are required in the construction of the embedding potential to ensure sufficient accuracy. The applicability of pseudopotentials in the calculation of kinetic energy potential contributions to the embedding operator was investigated in detail and a local truncation criterion on the conventional gradient expansion of the kinetic energy functional was introduced. A vertical excitation energy for the CO internal $^1(5\sigma/1\pi\rightarrow 2\pi^*)$ transition has been calculated in an embedded CASSCF/CI approach for the system CO/Pd(111), for which contradictory experimental results have been reported in the literature. We found the vertical excitation energy to be similar to the gas phase value, i.e., about 9 eV. Thus, our results corroborate the experimental findings for related systems such as CO/Fe(110), CO/Ni(100), and CO/Cu(100).[45,46]

The applicability of our embedding theory to electronically excited states is by no means straightforward, since the embedding operators are—at least partially—constructed from a DFT density, i.e., a theory based on the electronic ground state. A possible refinement could be realized in the following scheme:

(1) First, an embedding calculation for the electronic ground state would be performed to obtain the density in region I, $\rho_{\mathrm{I}}(\mathrm{GS})$.

(2) The density of region II, $\rho_{\mathrm{II}}(\mathrm{GS})$ is explicitly calculated by

$$\rho_{\mathrm{II}}(\mathrm{GS})=\rho_{\mathrm{tot}}(\mathrm{GS})-\rho_{\mathrm{I}}(\mathrm{GS}). \tag{18}$$

(3) If the cluster is sufficiently large, the density in region II is the same for ground and excited states, i.e.,

$$\rho_{\mathrm{II}}(\mathrm{GS})=\rho_{\mathrm{II}}(\mathrm{ES})=\rho_{\mathrm{II}}. \tag{19}$$

(4) Now, for excited states, state-averaged CASSCF calculations can be applied rigorously, so a state averaged density $\rho_{\mathrm{I}}(\mathrm{AV})$ can be obtained.

(5) Finally, $\rho_{\mathrm{tot}}(\mathrm{AV})$ and all embedding operators depending on $\rho_{\mathrm{I}}(\mathrm{AV})$ and $\rho_{\mathrm{tot}}(\mathrm{AV})$ can be updated by

$$\rho_{\mathrm{tot}}(\mathrm{AV})=\rho_{\mathrm{I}}(\mathrm{AV})+\rho_{\mathrm{II}}. \tag{20}$$

Future studies will provide insight into the advantage of this proposed refinement of our embedding scheme and will validate the approximations applied in the present work.

ACKNOWLEDGMENTS

Financial support from the U.S. National Science Foundation, the Air Force Office of Scientific Research, the Army Research Office, and the Deutsche Forschungsgemeinschaft is gratefully acknowledged.

[1] P. Sautet, M. K. Rose, J. C. Dunphy, S. Behler, and M. Salmeron, Surf. Sci. **453**, 25 (2000); D. Loffreda, D. Simon, and P. Sautet, *ibid.* **425**, 68 (1999); P. H. T. Philipsen, E. van Lenthe, J. G. Snijders, and E. J. Baerends, Phys. Rev. B **56**, 13 556 (1997); A. M. Bradshaw and F. M. Hoffmann, Surf. Sci. **72**, 513 (1978); M. Tüshaus, W. Berndt, H. Conrad, A. M. Bradshaw, and B. Persson, Appl. Phys. A: Solids Surf. **51**, 91 (1990); P. S. Bagus, C. J. Nelin, and C. W. Bauschlicher, Jr., Phys. Rev. B **28**, 5423 (1983); G. Pacchioni and J. Koutecký, J. Phys. Chem. **91**, 2658 (1987).

[2] (a) B. Hammer, L. B. Hansen, and J. K. Nørskov, Phys. Rev. B **59**, 7413 (1999); (b) J. P. Perdew, K. Burke, and M. Ernzerhof, Phys. Rev. Lett. **77**, 3865 (1996); A. D. Becke, J. Chem. Phys. **104**, 1040 (1996); **109**, 2092 (1998); **109**, 8188 (1998); M. Ernzerhof and G. E. Scuseria, *ibid.* **111**, 911 (1999); J. P. Perdew, S. Kurth, A. Zupan, and P. Blaha, Phys. Rev. Lett. **82**, 2544 (1999).

[3] (a) E. K. U. Gross and W. Kohn, Adv. Quantum Chem. **21**, 255 (1990); H. H. Heinze, A. Görling, and N. Rösch, J. Chem. Phys. **113**, 2088 (2000); M. E. Casida, F. Gutierrez, J. Guan, F.-X. Gadea, D. Salahub, and J.-P. Daudey, *ibid.* **113**, 7062 (2000); N. C. Handy and D. J. Tozer, J. Comput. Chem. **20**, 106 (1999); D. J. Tozer and N. C. Handy, Phys. Chem. Chem. Phys. **2**, 2117 (2000); M. Petersilka, U. J. Gossmann, and E. K. U. Gross, Phys. Rev. Lett. **76**, 1212 (1996); E. K. U. Gross, J. F. Dobson, and M. Petersilka, in *Topics in Current Chemistry*, edited by J. D. Dunitz *et al.* (Springer, Berlin, 1996), Vol. 181, p. 81, and references therein; S. Hirata, M. Head-Gordon, and R. J. Bartlett, J. Chem. Phys. **111**, 10774 (1999); M. Tobita, S. Hirata, and R. J. Bartlett, *ibid.* **114**, 9130 (2001). (b) K. Tatarczyk, A. Schindlmayr, and M. Scheffler, Phys. Rev. B **63**, 235106 (2001).

[4] (a) L. Hedin, Phys. Rev. A **139**, 796 (1965); M. S. Hybertsen and S. G. Louie, Phys. Rev. Lett. **55**, 1418 (1985); Phys. Rev. B **34**, 5390 (1986); R. W. Godby, M. Schlüter, and L. J. Sham, *ibid.* **37**, 10 159 (1988); M. Rohlfing, P. Krüger, and J. Pollmann, *ibid.* **52**, 1905 (1995); F. Aryasetiawan and O. Gunnarsson, Rep. Prog. Phys. **61**, 237 (1998); (b) M. Rohlfing and S. G. Louie, Phys. Rev. Lett. **81**, 2312 (1998); **82**, 1959 (1999); **83**, 856 (1999); Phys. Rev. B **62**, 4927 (2000); M. Rohlfing and J. Pollmann, *ibid.* **63**, 125201 (2001).

[5] J. Muscat, A. Wander, and N. M. Harrison, Chem. Phys. Lett. **342**, 397 (2001).

[6] For example, N. W. Ashcroft and N. D. Mermin, *Solid State Physics* (Saunders College, New York, 1976), pp. 334–337.

[7] D. Ceperley, G. Chester, and M. Kalos, Phys. Rev. B **16**, 3081 (1971).

[8] (a) W. M. C. Foulkes, L. Mitás, R. J. Needs, and G. Rajagopal, Rev. Mod. Phys. **73**, 33 (2001), and references therein; (b) J.-Q. Sun and R. J. Bartlett, J. Chem. Phys. **104**, 8553 (1996); Phys. Rev. Lett. **77**, 3669 (1996).

[9] I. Frank, J. Hutter, D. Marx, and M. Parrinello, J. Chem. Phys. **108**, 4060 (1998).

[10] J. C. Slater, Adv. Quantum Chem. **6**, 1 (1972); T. Ziegler, Chem. Rev. **91**, 651 (1991).

[11] E. Fattal, M. R. Radeke, G. Reynolds, and E. A. Carter, J. Phys. Chem. **101**, 8658 (1997); K. T. Queeney, Y. J. Chabal, and K. Raghavachari, Phys. Rev. Lett. **86**, 1046 (2001).

[12] T. Klüner, H.-J. Freund, V. Staemmler, and R. Kosloff, Phys. Rev. Lett. **80**, 5208 (1998); T. Klüner, S. Thiel, H.-J. Freund, and V. Staemmler, Chem. Phys. Lett. **294**, 413 (1998); S. Thiel, M. Pykavy, T. Klüner, H.-J. Freund, V. Staemmler, and R. Kosloff, Phys. Rev. Lett. **87**, 77601 (2001).

[13] T. Klüner, N. Govind, Y. A. Wang, and E. A. Carter, Phys. Rev. Lett. **86**, 5954 (2001).

[14] G. te Velde and E. J. Baerends, Chem. Phys. **177**, 399 (1993).

[15] (a) J. L. Whitten, J. Vac. Sci. Technol. A **17**, 1710 (1999); H. Nakatsuji, H. Morita, H. Nakai, Y. Murata, and K. Fukutani, J. Chem. Phys. **104**, 714

(1996); J. L. Whitten and H. Yang, Catal. Today **50**, 603 (1999); R. J. Buenker, H. P. Liebermann, and J. L. Whitten, Chem. Phys. **265**, 1 (2001); J. L. Whitten, J. Phys. Chem. B **105**, 4026 (2001); (b) Y. Fukunishi and H. Nakatsuji, J. Chem. Phys. **97**, 6535 (1992); H. A. Duarte and D. R. Salahub, *ibid.* **108**, 743 (1998); J. L. Whitten and T. A. Pakkanen, Phys. Rev. B **21**, 4357 (1980); I. V. Abarenkov, V. L. Bulatov, R. Godby, V. Heine, M. C. Payne, P. V. Souchko, A. V. Titov, and I. I. Tupitsyn, *ibid.* **56**, 1743 (1997); P. Cortona, *ibid.* **44**, 8454 (1991); J. R. Trail and D. M. Bird, *ibid.* **62**, 16402 (2000); D. E. Ellis, G. A. Benesh, and E. Byrom, J. Appl. Phys. **49**, 1543 (1978); T. N. Truong and E. V. Stefanovich, Chem. Phys. Lett. **240**, 253 (1995); T. A. Wesolowski and A. Warshel, J. Phys. Chem. **98**, 5183 (1993).

[16] N. Govind, Y. A. Wang, and E. A. Carter, J. Chem. Phys. **110**, 7677 (1999).

[17] N. Govind, Y. A. Wang, A. J. R. da Silva, and E. A. Carter, Chem. Phys. Lett. **295**, 129 (1998).

[18] An early attempt along similar lines used Hartree–Fock theory embedded in jellium—via the Green's function approach of Inglesfield [J. E. Inglesfield, J. Phys. C **14**, 3795 (1981)] —to examine an excited state of an Ar atom on a metal surface: A. N. Andriotis, Europhys. Lett. **17**, 349 (1992).

[19] T. Z. Mordasini and W. Thiel, Chimia **52**, 288 (1998); T. K. Woo, P. M. Margl, L. Deng, L. Cavallo, and T. Ziegler, Catal. Today **50**, 479 (1999); J. Sauer and M. Sierka, J. Comput. Chem. **21**, 1470 (2000); J. Gao, in *Encyclopedia of Computational Chemistry*, edited by P. von Ragué Schleyer *et al.* (Wiley, Chichester, 1998), Vol. 2, p. 1257, and references therein.

[20] M. Svensson, S. Humbel, R. D. J. Froese, T. Matsubara, S. Sieber, and K. Morokuma, J. Phys. Chem. **100**, 19357 (1996).

[21] A. D. Becke, J. Chem. Phys. **88**, 2547 (1988); A. D. Becke and R. M. Dickson, *ibid.* **89**, 2993 (1988).

[22] N. Troullier and J. L. Martins, Phys. Rev. B **43**, 1993 (1991).

[23] M. Dupuis, A. Marquez, and E. R. Davidson, HONDO 95.3 from CHEMStation, IBM Corporation, Neighborhood Road, Kingston, New York, 1995.

[24] P. Hohenberg and W. Kohn, Phys. Rev. B **136**, B864 (1964).

[25] M. Fuchs and M. Scheffler, Comput. Phys. Commun. **119**, 67 (1998).

[26] R. M. Dreizler and E. K. U. Gross, *Density Functional Theory* (Springer-Verlag, Berlin, 1990), p. 98.

[27] M. C. Payne, M. P. Teter, D. C. Allan, T. A. Arias, and J. D. Joannopoulos, Rev. Mod. Phys. **64**, 1045 (1992); CASTEP program, Accelrys, San Diego, CA.

[28] J. P. Perdew, J. A. Chevary, S. H. Vosko, K. A. Jackson, M. R. Pederson, D. J. Singh, and C. Fiolhais, Phys. Rev. B **46**, 6671 (1992).

[29] (a) H. Ohtani, M. A. van Hove, and G. A. Somorjai, Surf. Sci. **187**, 372 (1987); (b) P. J. Hay and W. R. Wadt, J. Chem. Phys. **82**, 270 (1985).

[30] W. J. Stevens, H. Basch, and M. Krauss, J. Chem. Phys. **81**, 6026 (1984).

[31] Pd: $3s3p4d/2s2p2d$ from Ref. 29; C,O: $4s4p/2s2p$ from Ref. 30 augmented by $1d(0.8)+1p(0.05)$. The numbers in parentheses denote the exponents of the additional basis functions.

[32] S. F. Boys and F. Bernardi, Mol. Phys. **19**, 553 (1970).

[33] Q. Zhao and R. G. Parr, J. Chem. Phys. **98**, 543 (1993); A. Görling and M. Ernzerhof, Phys. Rev. A **51**, 4501 (1995).

[34] MOLCAS, Version 4, K. Andersson, M. R. A. Blomberg, M. P. Fülscher *et al.* (Lund University, Sweden, 1997).

[35] T. H. Dunning, Jr., J. Chem. Phys. **53**, 2823 (1970); T. H. Dunning, Jr. and P. J. Hay, in *Methods of Electronic Structure Theory*, edited by H. F. Schaefer III (Plenum, New York, 1977), Vol. 2.

[36] R. A. Kendall, T. H. Dunning, Jr., and R. J. Harrison, J. Chem. Phys. **96**, 6769 (1992).

[37] T. H. Dunning, Jr., J. Chem. Phys. **90**, 1007 (1989).

[38] H. Conrad, G. Ertl, J. Koch, and E. E. Latta, Surf. Sci. **43**, 462 (1974); X. Guo and J. T. Yates, Jr., J. Chem. Phys. **90**, 6761 (1989).

[39] Y. A. Wang and E. A. Carter, in *Theoretical Methods in Condensed Phase Chemistry*, edited by S. D. Schwartz, within the series *Progress in Theoretical Chemistry and Physics* (Kluwer, Dordrecht, 2000), p. 117.

[40] Q. Zhao, M. Levy, and R. G. Parr, Phys. Rev. A **47**, 918 (1993).

[41] J. A. Alonso and L. A. Girifalco, Phys. Rev. B **17**, 3735 (1978).

[42] K. P. Huber and G. Herzberg, *Molecular Spectra and Molecular Structure IV. Constants of Diatomic Molecules* (Van Nostrand, Reinhold, New York, 1979).

[43] J. Zobel, U. Mayer, K. Jung, and H. Ehrhardt, J. Phys. B **29**, 813 (1996); P. H. Krupenie, Natl. Stand. Ref. Data Ser. **5**, 1 (1966), S. G. Tilford and J. D. Simmons, J. Phys. Chem. Ref. Data **1**, 147 (1972).

[44] F. P. Netzer and M. M. El Gomati, Surf. Sci. **124**, 26 (1983).

[45] H.-J. Freund, R. P. Messmer, W. Spiess, H. Behner, G. Wedler, and C. M. Kao, Phys. Rev. B **33**, 5228 (1986).

[46] Ph. Avouris and J. E. Demuth, Surf. Sci. **158**, 21 (1985).

[47] Due to large mixing of the CO and Pd orbitals in a state-averaged scheme, the excitation energy of the nonembedded Pd_6/CO cluster has been obtained by optimizing the orbitals of each state separately. Therefore it cannot be compared directly with state-averaged results reported in Table VI.